J MATER RES TECHNOL. 2019;8(2):1701–1711

Available online at www.sciencedirect.com

jmr&t Journal of Materials Research and Technology

www.jmrt.com.br

Original Article

Application of response surface methodology for optimization of hybrid friction diffusion bonding of tube-to-tube-sheet connections in coil-wound heat exchangers

Diego Rafael Alba[a,*,1], *Arne Roos*[a], *Georg Wimmer*[b], *Arnaldo Ruben Gonzalez*[a,2], *Stefanie Hanke*[a,3], *Jorge Fernandez dos Santos*[a]

[a] *Helmholtz Zentrum Geesthacht, Centre for Materials and Coastal Research, Materials Mechanics, Solid State Joining Processes, Max-Planck-Strasse 1, 21502, Geesthacht, Germany*

[b] *LINDE AG, Engineering Division, Werk Schalchen, Carl-von-Linde-Strasse 15, 83342, Tacherting, Germany*

ARTICLE INFO

Article history:
Received 16 February 2018
Accepted 14 November 2018
Available online 17 January 2019

Keywords:
Solid state welding
Hybrid friction diffusion bonding
5XXX series aluminum
Box–Behnken design
Response surface methodology

ABSTRACT

This study evaluates the application of a new solid state joining process referred to as hybrid friction diffusion bonding. Based on heat processing and pressure, accelerated diffusion joins the materials. In the present study, two aluminum alloys were welded and characterized using leak tightness tests, tensile pull out tests, and metallographic analysis. Response surface methodology was used to optimize the tensile strength of single-hole tube-sheet samples. A Box–Behnken design was selected to evaluate the relations between the important process parameters and the ultimate tensile strength response to obtain optimal welding parameters. The data were analyzed with analysis of variance and were fitted to a second-order polynomial equation. The three-dimensional response surfaces derived from the mathematical models were applied to determine several optimum input parameters conditions. Under these conditions, the experimental ultimate tensile strength value was 202 MPa, which represents 95% of the base material strength. The experimental results obtained under optimum operating conditions were in agreement with the predicted values. Axial force was found to be the most significant factor affecting the joint strength followed by rotational speed. This can be attributed to their influence on the amount of mechanical energy introduced during the process, which is the parameter that primarily determines the joint strength.

* *Corresponding author.*
E-mails: diego.alba@ufrgs.br, eng.diego.alba@gmail.com (D.R. Alba).
[1] Address: Federal University of Rio Grande do Sul, PPGE3M, Bento Gonçalves Avenue 9500, 91501, Porto Alegre, Brazil.
[2] Address: Federal University of Rio Grande do Sul, PROMEC, Sarmento Leite Street 425, 90050, Porto Alegre, Brazil.
[3] Address: Duisburg-Essen University, Institute for Metals Technology, Lotharstrasse 1, 47057, Duisburg, Germany.

https://doi.org/10.1016/j.jmrt.2018.11.012

1. Introduction

The coil-wound heat exchanger (CWHE) is central and critical to the operations of the liquefied natural gas (LNG) plant, where natural gas is liquefied and subcooled. Since the early days of LNG, CWHE technology has continued to evolve in order to meet industrial requirements. One of the challenges during the manufacturing of the CWHE refers to the joints between the tubes and the tube sheets, which seal the LNG from the environment. Each tube sheet in industrial heat exchangers contains hundreds of holes, depending on the size of the respective unit, into which tubes are welded, e.g., by tungsten inert gas (TIG) welding. Challenges in the manufacturing of these complex components with the use of conventional joining techniques include the low-permissible tolerances, limited possibilities of automation, the risk of pore formation, or welding defects leading to leakage. New technologies, which are less labor-intensive and time consuming, are sought to address these challenges. Hybrid friction diffusion bonding (HFDB) is an innovative technology, and its feasibility in producing tube-to-tube sheet joints of exceptional quality has already been shown in previous publications [1]. In the current work, the process parameters of HFDB for CWHE from 5000 series aluminum alloys were optimized based on the statistical design of experiments. Furthermore, the significance of the main process parameters on the achieved joint strength was evaluated using analysis of variance (ANOVA), and was correlated with process temperatures and the energy input into the weld region. The aim of this work is to gain a deeper understanding of the mechanisms determining the joint formation and strength, in order to advance the applicability of this promising technology.

HFDB process was developed and patented at the German research center *Helmholtz Zentrum Geesthacht*, and was first described by Roos [2,3]. This process combines the advantages of diffusion bonding and friction welding. The new method was initially developed for producing joints with dissimilar overlaps and butt joint connections of thin sheets, and for joining thin sheets onto substrates. Further information regarding the standard process can be found in the work of Roos [2] and Bergmann et al. [4]. A variant of the standard process was developed for joining tubes and tube-sheets for the manufacturing of heat exchangers [1,5].

Fig. 1 schematically shows the basic design of an HFDB tool for CWHE applications. The effective contact area of the tool consists of a planar friction area (PFA) and a conical friction area (CFA). The tools may have a spiral feature at the planar friction area to facilitate material flow. For example, it is possible to vary both the diameter of the planar friction area as well as the angle of the conical friction area. For the work at hand, the tool material is a hot working tool steel.

In the execution of this process, the tool is rotated at a speed of n (min^{-1}). An axial force F (kN) is then applied. Fig. 2 illustrates the division of the bonding process into two main stages. During the insertion phase, initially only the conical friction area of the rotating tool is in contact with the inner surface of the tube, as indicated by Fig. 2b. The resulting friction generates heat and shear stresses, and the tube material in contact with the tool begins to undergo plastic shear deformation in the circumferential direction. Moreover, the conical friction area of the tool, which has a larger diameter than the inner diameter of the tube, exerts radial pressure onto the inner wall of the tube, thus resulting in plastic deformation and the transfer of the pressure onto the inner surface of the tube-sheet bore.

Subsequently, during the welding phase, both the planar and conical friction areas are in contact with the workpiece, as shown in Fig. 2c. Full contact between the tool and the workpiece generates an increased amount of heat, which in combination with the applied pressure joins the tube and the tube sheet based on the diffusion processes in the contact zone. It has been shown by Dethlefs [1] and Roos et al. [6] that the thermal softening and plastic material flow of both the tube material interacting with the conical friction area, and the tube-sheet material close to the planar friction area, result in dynamic recrystallization. The state of the material with which it reaches during the HFDB process is referred to as “plasticized.” Finally, the rotating tool is withdrawn after a preset welding time.

The Box–Behnken design (BBD) was first proposed by Box and Behnken [7] and became a useful design for experiments conducted with the response surface methodology (RSM) for industrial process development and optimization, as well as product design. BBD is a convenient method used for developing second-order response surface models [7,8]. BBD constitute an alternative to central composite designs. They are a class of rotatable or nearly rotatable second-order

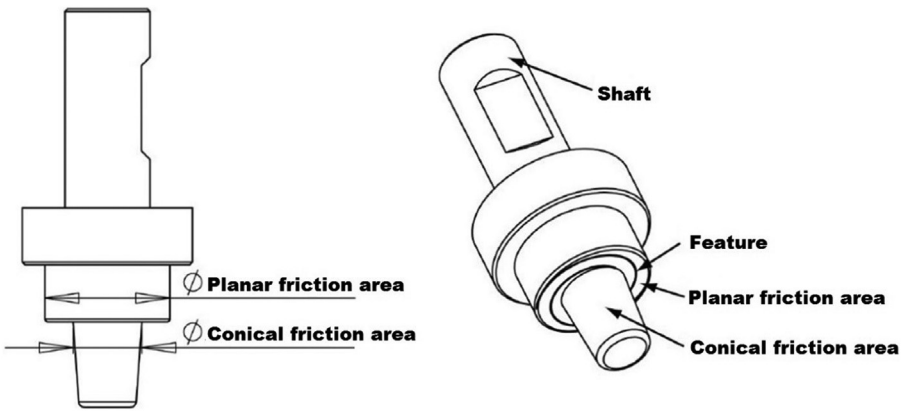

Fig. 1 – Schematic illustration of an HFDB tool for joining CWHE tubes to tube sheets.

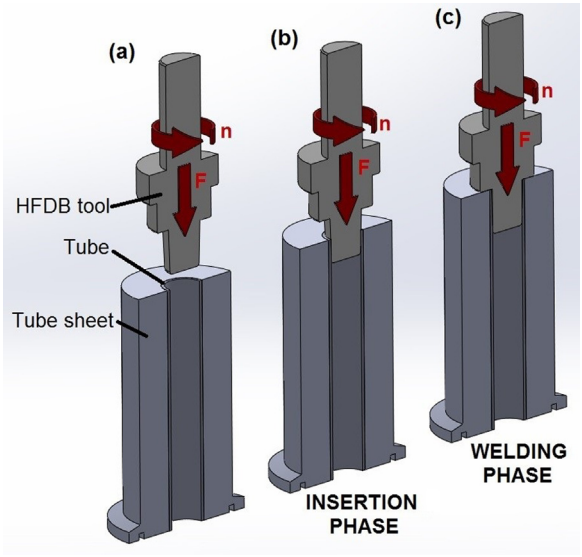

Fig. 2 – Schematic drawing showing the HFDB for CWHE application. (a) Pre-positioning and rotating of the tool, (b) insertion phase and (c) welding phase.

designs based on three-level incomplete factorial designs. More information on the properties of BBD can be found in the literature [7,9,10]. The use of BBD is widespread in industrial research because of its cost-effectiveness, since it requires only three levels for each factor. Another advantage is that it does not contain combinations where all the factors are in the highest or lowest levels. In that way, the experiments are not performed under extreme conditions.

One of the main objectives of the BBD method is the determination of the optimum settings of the controlled factors that result in a maximum (or minimum) response over the experimented region. To achieve this, it is required that the proposed model has a good fit with the experimental values. ANOVA is a statistical tool used to test the equality of several population means, i.e., it investigates the degrees of differences or similarities between two, or among more groups of data. It employs sum-of-squares and F-statistics to predict the fit of the model and to discover the significance of each factor in regard to the elicited response. As the last step, fitting a second-order model to the response variable(s) of interest is an integral aspect of RSM. The method of least-squares is typically utilized to estimate the regression coefficients [9,11].

Modeling is typically conducted by fitting simple models (linear or quadratic, as a rule) to response values obtained from standard or augmented factorial designs. The use of well-structured optimization procedures to improve a certain process serves to reduce time and the number of experiments needed. A search for significant effects related to the various factors on quality parameters is demanding, and in this context, the BBD used to study three independent variables followed by RSM, is a tool that helps estimate the influences of variables on the process. Furthermore, these tools are useful to optimize the process conditions (i.e., torque, temperature, energy input, etc.) in order to obtain an improved (variable response) product or process.

2. Experimental procedure

For this work, base materials (BMs) for the CWHE HFDB samples consisted of two dissimilar alloys from the aluminum 5000 series. The 5000 series aluminum alloys contain magnesium as the main alloy element, and both types of materials have been used for cryogenic applications in pressure vessels according to the AD2000 standard [12]. The main properties of the 5000 series aluminum alloys are moderate strength, good weldability, and good corrosion resistance. The composition range of both 5000 series aluminum alloys used in this work is shown in Table 1.

For the characterization of the BM strength, five tubes were subjected to tensile tests. Plugs were inserted into the ends of the tubes to prevent them from collapsing under the clamping force. The average of the tensile strength of the base material was considered as the base material strength for the remainder experiments of this study. The average value of the BM tensile fracture force was 10.2 kN with a standard deviation of 261 N (2.6%). To calculate the tensile strength, the cross-section of the tube was considered as the effective area, which resulted in a ultimate tensile strength (UTS) value for the BM tubes of 211 MPa. According to the AD2000 standard [12], the minimal value of the UTS for the tube is 180 MPa. Correspondingly, elicited results show that the measured values for the material used to conduct the HFDB experiments was in accordance to the standard's requirements.

As previously described, for industrial applications, a single tube sheet may contain hundreds of tube holes. For understanding the process as well as the behavior of the welds carried out during the parameter tests, single-hole tube sheet dummies were used. This is cost effective as well as time saving for an experimental study. A schematic sketch of the dimensions of both the tube sheet dummies as well as the tubes for HFDB of the CWHE is shown in Fig. 3. To facilitate the integration into the clamping system, the length of the tubes was 180 mm.

All samples were thoroughly cleaned before each experiment. The cleaning procedure consisted of grinding the welding area with SiC grinding paper with ISO grit size of 800. Subsequently, the samples were immersed in acetone and were left in an ultrasonic bath for 5 min. In addition, a pneumatic tool was used to expand the tubes into the tube sheets after the sample was mounted, thus improving the initial contact between the tube and the tube-sheet dummy.

Table 1 – Base material chemical composition.

Material	Mg [%]	Fe [%]	Si [%]	Ti [%]	Mn [%]	Cu [%]	Al [%]
AA 5XXX tube and tube sheet	1.6–4.9	0.4–0.5	≤0.4	0.1–0.15	0.4–1.1	≤0.1	92.4–97.9

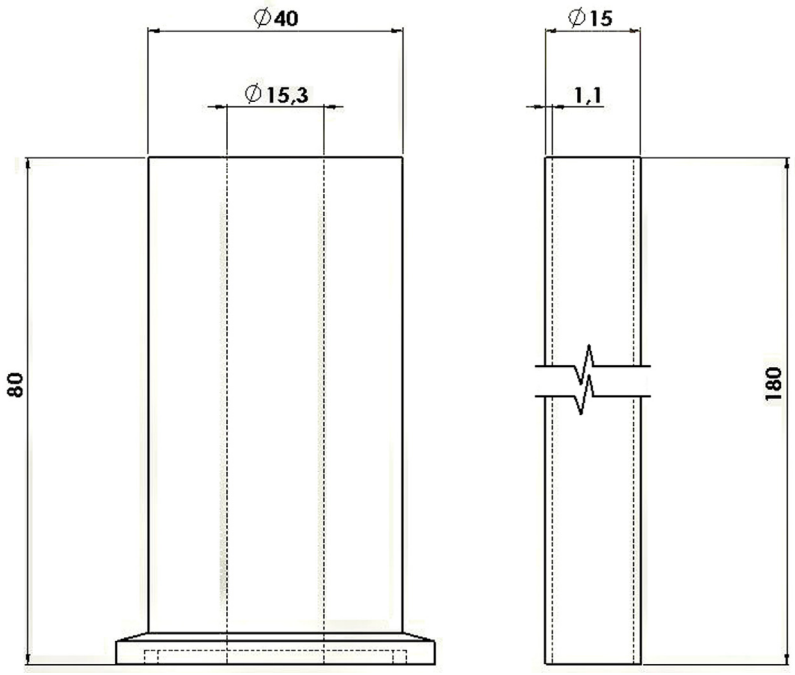

Fig. 3 – Drawings of single hole tube sheet dummy and tube geometries for investigation of HFDB in CWHE.

Table 2 – HFDB CWHE process parameters; natural and coded levels.

Factor		Level		
Independent variables	Notation	−1 (low)	0 (center)	+1 (high)
Rotational speed [min^{-1}]	RS	1000	1500	2000
Axial force [kN]	AF	2	2.5	3
Process time [s]	PT	30	35	40

The three factors were evaluated in this study based on the Box–Behnken design, i.e., rotational speed (RS in min^{-1}), axial force (AF in kN), and process time (PT in seconds) were varied based on previously executed process feasibility studies [1,2,6]. Table 2 shows each analyzed factor as well as the evaluated levels.

3. Characterization

To measure the leak tightness of the joints, a bubble test apparatus in accordance with DIN EN 1593 (1999–11) was used [13]. To perform this test, the free end of the tube was sealed with a plug, and the flange of the welded sample was clamped onto the pressure cylinder. The pressure cylinder and the inner volume of the welded sample were then pressurized to 300 kPa. When the sample was pressurized, a test fluid was sprayed onto the welded zone. According to the standard, the leakage rate can be estimated from the size and number of bubbles per unit time. If no more than one bubble with a diameter of 1 mm appears at every 10 s, the sample is considered leak tight in the welded area up to a leak rate of 10^{-6} kPa l/s.

For metallographic examination, transverse sections of the welded samples were cut, ground, and polished. All samples used for the optical microscopic analyses were prepared following a standard metallographic procedure for aluminum preparation. The samples were then electrolytically etched with Barker's solution at 30 V for 150 s. The analyses were carried out with polarized light using an Olympus PMG 3 optical microscope.

To determine the quasistatic mechanical performance of the welded CWHE HFDB samples, tensile pull out tests were performed on a Zwick 1734 universal testing machine. Fig. 4 shows a schematic depiction of the tensile test. The welded samples were fixed on special clamping jaws designed for cylindrical workpieces. A cylindrical plug was inserted into the open end of the tube to stiffen the tube against the clamping forces and to avoid the distortion of the tube. The tensile pull out rate imposed during the test was 1 mm/min.

The temperature of the process was measured with K-type thermocouples with a diameter of 0.5 mm positioned as close as possible to the joining area. The position of the thermocouples is shown schematically in Fig. 5. The holes with a diameter of approximately 0.5 mm were manufactured by spark erosion drilling. During the HFDB experiments, a high-conductivity thermal compound was used to enable a better contact, thus ensuring precise temperature measurements.

4. Results and discussion

The fifteen required experiments for the BBD analysis were performed and Fig. 6 shows a set of three samples welded by HFDB. As can be seen, the different input parameters for each experiment influences the flash geometry of the weldments. Posteriorly, all welded samples underwent the bubble leak tightness test and no bubbles were observed. Thus, the samples were considered leak tight with an estimated leakage rate of at most 10^{-6} kPa l/s. Leak rate is considered the most

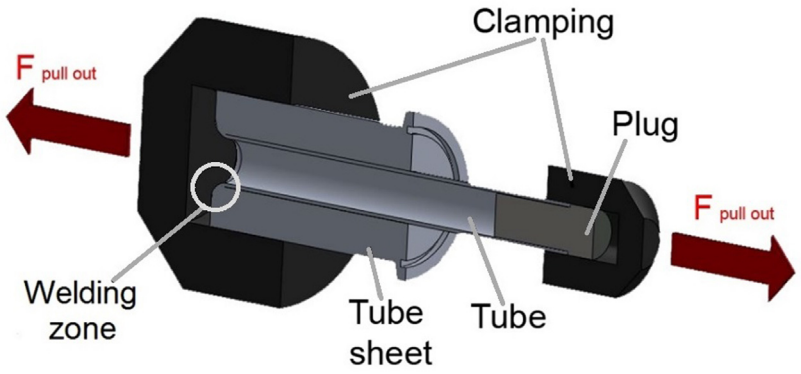

Fig. 4 – Schematic setup for tensile pull-out tests of single hole tube to tube-sheet HFDB joints. The plug prevents tube collapse during testing.

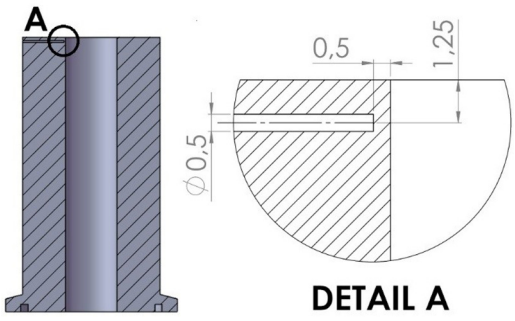

Fig. 5 – Thermocouples position on the HFDB tube to tube sheets experiments.

important criterion for the CWHE application. This criterion was achieved and it was not affected by any of the process parameters under consideration.

For the microstructural characterization, the samples were polished, etched, and analyzed under polarized light, as previously described. Fig. 7 shows a typical microstructure of an HFDB tube-to-tube sheet joint. The welded zone can be divided into three main areas. The thermo-mechanically affected zone (TMAZ) underwent plastic deformation and high-process temperatures, and can be characterized by the existence of fine grains owing to dynamic recrystallization. Adjacent to this zone, the heat affected zone (HAZ) is present where only a rise in temperature occurred and a transition from fine equiaxed grains (as in the TMAZ) to elongated grains could be observed. Next to the HAZ, the unaffected BM was located where no microstructural changes occurred, and where the grains maintained their elongated shape and the size generated during the cold work production phase of the base material [1,2,14,15].

One of the main advantages of solid state joining processes is the relatively low-heat input required, which avoid conversion of the state of the materials to a liquid form. The small HAZ that results can be observed in Fig. 7. It extends to approximately 3–5 mm below the contact area of the tool's planar friction area. In addition, the area beside the flash formed during the process is not affected, thus showing that the heat dissipation occurs mainly in the direction of the largest mass of the sample.

In relation to the tensile test results, the results from the fifteen runs required for the BBD using three factors as well as the geometric notation for the design of experiments are shown in Table 3. The running order was randomized before the onset of the experiments. The response of the variable UTS (MPa), was also evaluated, as listed in the table. Table 3 further presents the results related to the maximum temperature and energy input, which will be later discussed in this work. Failure always occurs in the tubes below the joining area, as already described in Dethlefs [1] and Roos et al. [6], thus allowing a direct comparison with the BM strength of the tube, as described in Section 2. It can be observed that the variation in the UTS of the joints is in a range of 50 MPa, with two thirds of the runs resulting in UTS values above 190 MPa, and three samples reaching values higher than 200 MPa, which are close to the BM strength of 211 MPa.

Based on the obtained values, a second-order (or regression) model for predicting the UTS was devised. To verify the adequacy of the model, the coefficient of determination R^2 was evaluated. The closer this coefficient is to a value of 1, the better is the adequacy of the model. The R^2 value provides

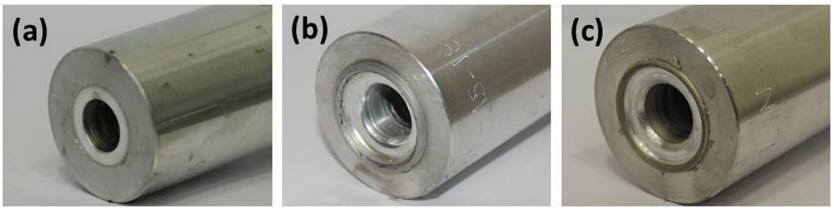

Fig. 6 – Welded samples by HFDB; (a) RS = 1000 s^{-1}, AF = 2 kN, PT = 35 s; (b) RS = 2000 s^{-1}, AF = 3 kN, PT = 35 s; (a) RS = 1500 s^{-1}, AF = 2.5 kN, PT = 35 s.

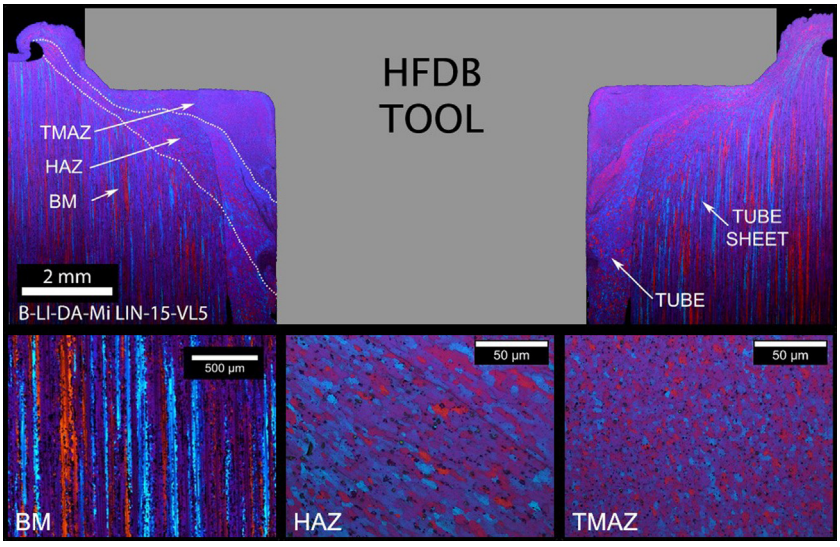

Fig. 7 – Metallographic cross section showing the different regions of a HFDB CWHE welded specimen.

Table 3 – Design matrix for analysis and results of pull-out tests, maximum temperature and energy input of the weldments.

Run	Standardized coded factor			Rotational speed [min^{-1}]	Axial force [kN]	Process time [s]	Pull out stress [MPa]	Maximum temperature [°C]	Energy input [kJ]
1	−1	−1	0	1000	2	35	142	395	56
2	−1	1	0	1000	3	35	178	490	75
3	1	−1	0	2000	2	35	175	520	98
4	1	1	0	2000	3	35	195	568	114
5	0	−1	−1	1500	2	30	156	464	64
6	0	1	−1	1500	3	30	199	490	78
7	0	−1	1	1500	2	40	189	479	82
8	0	1	1	1500	3	40	198	495	108
9	−1	0	−1	1000	2.5	30	190	454	63
10	1	0	−1	2000	2.5	30	199	559	88
11	−1	0	1	1000	2.5	40	190	470	80
12	1	0	1	2000	2.5	40	198	549	114
13	0	0	0	1500	2.5	35	205	508	92
14	0	0	0	1500	2.5	35	206	506	88
15	0	0	0	1500	2.5	35	204	509	96

a measure of variability in the observed response values and can be explained by the factors and their interactions. For this set of experiments, the calculated value of R^2 was 0.942. Therefore, it can be concluded that 94.2% of the observed variability in tensile strength could be explained by the independent variables. To further ensure the adequacy of the model it is possible to compare the observed and the predicted values. In the diagram in Fig. 8, the predicted values are shown as a line plot, and the observed values as dots. The closer the observed values are to the predicted values, the better is the adequacy of the developed model.

One of the main reasons for performing an ANOVA is to understand the factors that are more relevant to the process and the interactions among them. The criteria followed in this technique are based on the fact that if the calculated value of the *F*-ratio in the regression model is higher compared to the standard value specified on the *F*-table for the 95% confidence level, the interaction is considered relevant and adequate within the confidence limit. To avoid the necessity to compare the *F*-value calculated with the *F*-value from the table, the *p*-value was analyzed. If the *p*-value was below 0.05 (i.e., for a 95% confidence level), the interaction was considered relevant. Table 4 shows the ANOVA results based on the conducted experiments.

By analyzing the ANOVA (see Table 4), and considering the Pareto chart (see Fig. 9), the axial force (linear (L) and quadratic (Q) terms) were found to be significant with a contribution of 62.8%. By increasing this factor, it is possible to increase the ultimate tensile pull out strength within the investigated parameter range. The linear and quadratic terms of the rotational speed (contribution of 22.8%) have a significant effect on the ultimate tensile pull out strength, while the other factors and their interactions have no significant effects on the evaluated response (their total contribution was 10.4%).

A mathematical model known as a regression model characterizes the relationship between the independent variables

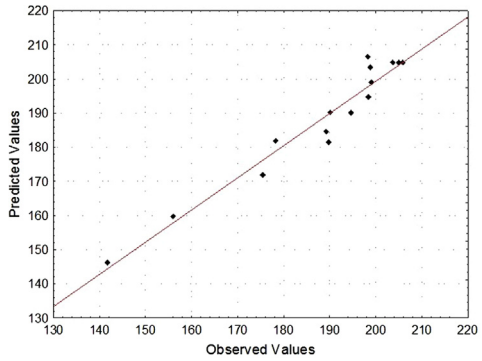

Fig. 8 – Comparison of predicted ultimate tensile pull out strength with experimental data from HFDB CWHE tube to tube sheet welds.

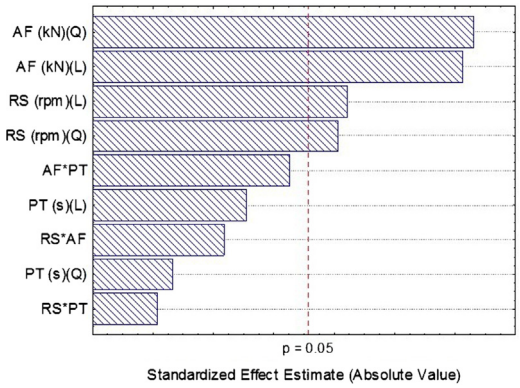

Fig. 9 – Pareto chart of standardized effects in CWHE HFDB of tube to tube sheets; variable: UTS (MPa).

and the elicited response. Based on the above analysis, it is possible to obtain a model to predict the ultimate tensile pull out strength over the experimental region.

Furthermore, a regression analysis was performed to fit the response variable. The resulting second-order polynomial equation, adjusted at a 95% of confidence level, represents response variables as functions of axial force, rotational speed, and process time. Table 5 shows all coefficients of the regression equation as well as each respective standard error. After the ANOVA analysis, all factors that did not have relevance to the model were disregarded. Eq. (1) can express an empirical relationship between the response and the significant input test variables.

Table 5 – Regression coefficients for UTS response of CWHE HFDB experiments in the studied parameter window.

Factor	Regression coefficient
Constant	−837.597
Rotational speed (linear)	20.621×10^{-2}
Rotational speed (quadratic)	-47.250×10^{-6}
Axial force (linear)	580.607
Axial force (quadratic)	−81.999
Process time (linear)	5.801
Process time (quadratic)	51.039×10^{-3}
Rotational speed × axial force	-17.445×10^{-3}
Rotational speed × process time	-11.242×10^{-5}
Axial force × process time	−3.358

$$\hat{\sigma} = -837.597 + 580.607AF + 20.621 \times 10^{-2}RS - 81.999AF^2 - 47.250 \times 10^{-6}RS^2 \quad (1)$$

where $\hat{\sigma}$ is the ultimate tensile strength in MPa, AF is the axial force in kN and RS is the rotational speed in min^{-1}.

Based on the regression equation, the three-dimensional surface plots for the response in terms of the rotational speed and axial force of the process variables at different process times are shown in Figs. 10–12. The process time was kept constant since it was the process parameter with the least influence on the response during the experiments. It is relatively easy to notice from examining these figures that the optimum values are approximately equal to 1700 min^{-1} and 2.5 kN for a process time of 40 s, and that the response is at its maximum at this point. From the examination of these plots, it is clear that the process may be slightly more sensitive to changes in the axial force than to changes in rotational speed.

It can be observed that based on the model's prediction, response values above 210 MPa are achievable, although none of the experiments reached such high values. As previously described, the prediction of the model fits well the measured values for the calculated regression equation. Owing to the variance and error of the model, it is not possible to ensure

Table 4 – ANOVA table for UTS response showing the values used to analyze the relevance of each factor and to define a regression analysis for the HFDB CWHE tube to tube sheet process.

Factor (source)	Sum of squares	Degree of freedom	Mean square	F-calculated	*p*-value	Effect	Contribution (%)
RS [min^{-1}] (L)	571.516	1	571.516	10.372	0.023	Significant	11.97
RS [min^{-1}] (Q)	515.29	1	515.290	9.352	0.028	Significant	10.79
AF [kN] (L)	1448.58	1	1448.590	26.291	0.003	Significant	30.34
AF [kN] (Q)	1551.66	1	1551.670	28.162	0.003	Significant	32.50
PT [s] (L)	131.330	1	131.330	2.384	0.183	No-Signif.	2.75
PT [s] (Q)	6.010	1	6.010	0.109	0.754	No-Signif.	0.13
RS (L) by AF (L)	76.090	1	76.090	1.381	0.292	No-Signif.	1.59
RS (L) by PT (L)	0.316	1	0.316	0.0057	0.942	No-Signif.	0
AF (L) by PT (L)	281.900	1	281.900	5.116	0.073	No-Signif.	5.90
Error	275.490	5	55.098				
Total sum of squares	4774.06	14					

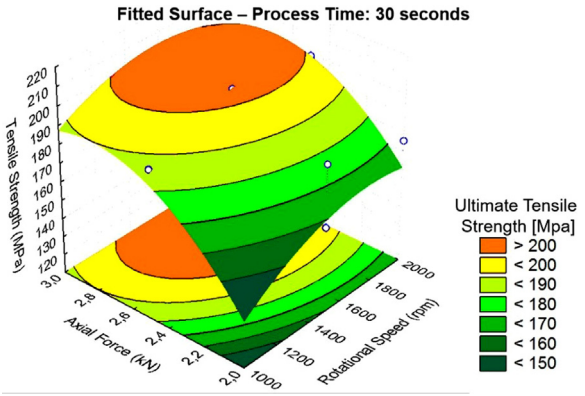

Fig. 10 – 3D surface plot for the response in terms of the process variables rotational speed and axial force for a process time of 30 s.

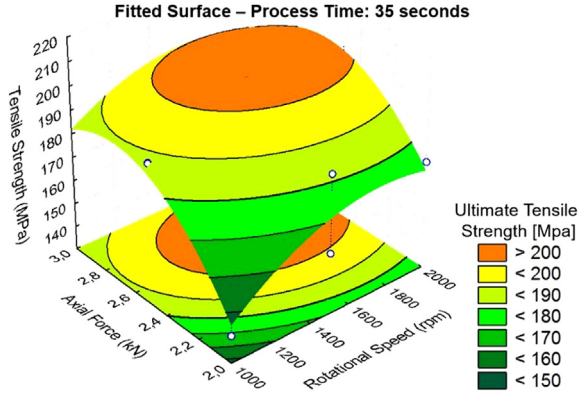

Fig. 11 – 3D surface plot for the response in terms of the process variables rotational speed and axial force for a process time of 35 s.

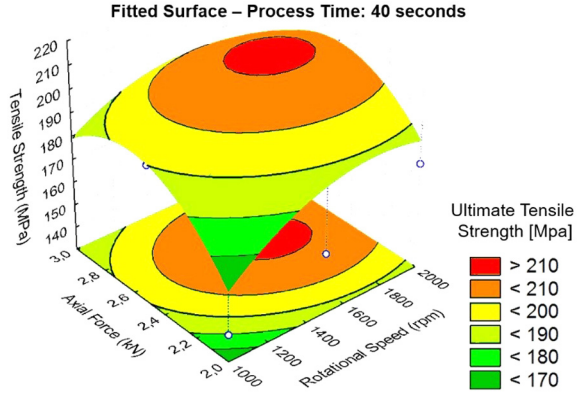

Fig. 12 – 3D surface plot for the response in terms of the process variables rotational speed and axial force for a process time of 40 s.

that such results could be achieved, but at least it is shown that this is the optimized area of the investigated parameter window.

In addition to the verification based on ANOVA, the regression model was validated by conducting experiments with new sets of parameters. The response values were measured

Table 6 – CWHE HFDB parameters set chosen for regression model validation.

Parameter	Set 1	Set 2
Rotational speed [min^{-1}]	1600	1500
Axial force [kN]	2.8	3.0

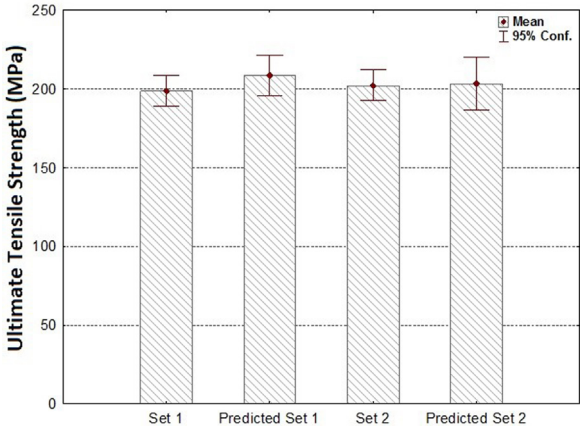

Fig. 13 – Ultimate tensile pull out strength response of the welded HFDB CWHE samples for validation of the regression model.

and compared with the prediction of the model shown in the previous section. The CWHE HFDB process parameters chosen for validation are presented in Table 6 and arise from Fig. 11. A process time of 30 s has been chosen in view of the higher efficiency required in industrial applications. For the validation of the model, three experiments for each set were performed.

The tensile pull out strength results are presented in Fig. 13, whereby the maximum strength for each parameter set and its variance for a confidence level of 95% are shown.

The prediction using the regression model is in accordance to the results from the validation experiments. The predicted sets for both experimental conditions presented a larger variance than that elicited by the experiments. Based on the use of the regression equation it is possible to vary the process parameters (mainly AF, RS) to estimate the average value of the response (UTS) and its variance. As expected, small variations in the elicited results could be observed, but the latter did not void the robustness of the process. The optimized parameter set 1 reached 94% of the BM tensile pull out strength, while parameter set 2 reached 95%. Irrespective of the range of scatter for each set, they both yielded the same joint strength.

For a better understanding of the mechanical performance of the weldments, a correlation between the input parameters and temperatures with its UTS is necessary. Firstly, as stated by Roos et al. [6] and Dethlefs [1], the fracture of the weldments occurs in the HAZ of the tubes in an area below the bonding zone. Both studies suggest notch effects due plastic deformation developed during the joining as well as the softening of the material owing to the recovery and grain growth in the undeformed HAZ as the possible factors that influence the failure location. The latter would be related to the increased process temperatures.

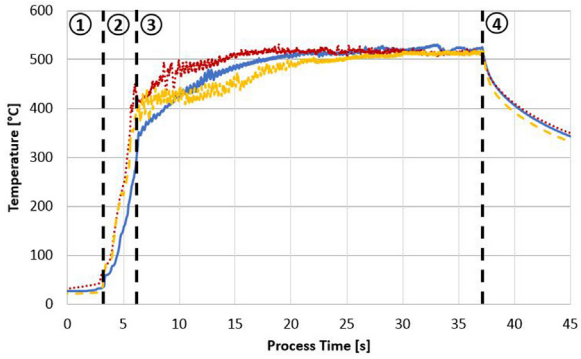

Fig. 14 – Typical temperature curve of a HFDB tube to tube sheet showing the four stages of the process.

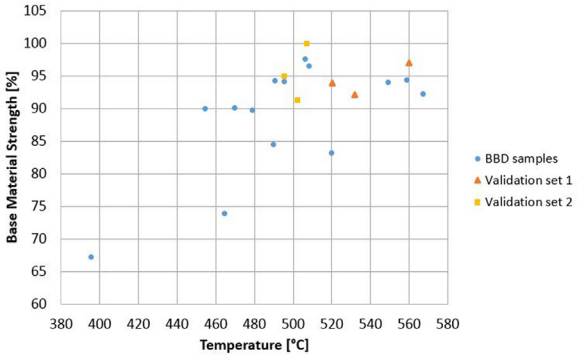

Fig. 15 – Maximum process temperatures and resultant UTS of the weldments in relation to the base material strength.

As shown by the Box–Behnken design analysis, the parameters that most influence the mechanical performance of the weldments are the axial force (62.8%) and rotational speed (22.8%). Thus, it can be concluded that the differences in the process time are too small to significantly affect the softening effect of the increased temperatures in the HAZ.

Process temperatures were measured as previously described during all experiments for the BBD and validation investigation. Maximum process temperatures varied from 460 °C to 560 °C depending on the chosen process parameters. Fig. 14 shows the characteristic temperature curve for the three samples of the validation set 1. During the advancing stage (region 1) of the tool, the first cycle of frictional heat is generated when the conical friction area of the tool touches the inner part of the tube. When the planar friction area of the tool touches the tube sheet (region 2), a larger frictional area is created. In this phase, an abrupt heating effect at temperatures above 400 °C is measured. Lastly, a further increase in the process temperature is noted, and an upper temperature limit is reached (region 3). Heat generation in the HFDB only partially occurs owing to friction. At high temperatures, it can be assumed that the main source of heat is viscous dissipation during the plastic material flow. Since the shear stress acting on the deforming material decreases as the temperature rises, the amount of heat produced in the process declines. To balance this with the heat flowing into the sample and the surroundings, the temperature attains a constant value. The tool is then withdrawn and natural cooling takes place (region 4).

Fig. 15 depicts maximum process temperatures and corresponding UTS values of all conducted welds. A trend is visible that it is necessary to reach a temperature above approximately 450 °C to achieve a weldment with good properties. With further increases in the process temperature, the scatter of the results decreases and the measured values range between 90 and 100% of the base material strength. Still, there is no evident correlation between the process temperature and weldment strength. For example, welds with a difference in the maximum temperature by approximately 100 °C may vary by less than 2% in terms of their UTS values when compared to the base material. Therefore, it can be concluded that high process temperatures are not detrimental to the joint properties, and the softening of the HAZ may occur to a comparable degree for parameter values in the range investigated in the current study.

Aiming to a better understanding of the temperature development during the experiments, and in accordance to the same procedure as that used for UTS analysis, an ANOVA test of the maximum achieved temperatures was performed. The results of the ANOVA test are shown in Table 7. Subsequently, it is possible to define the parameters that are significant for the analyzed response. Rotational speed with 70.17% followed by axial force increases with 21.40% are the parameters that significantly affect the maximum temperature reached during

Table 7 – ANOVA table for maximum temperature response showing the values used to analyze the relevance of each factor for the HFDB CWHE tube to tube sheet process.

Factor (source)	Sum of squares	Degree of freedom	Mean square	F-calculated	*p*-value	Effect	Contribution (%)
RS [min^{-1}] (L)	18,663.1	1	18,663.1	71.32	0.000	Significant	69.73
RS [min^{-1}] (Q)	119.3	1	119.3	0.46	0.530	No-Signif.	0.44
AF [kN] (L)	4250.4	1	4250.4	16.24	0.010	Significant	15.88
AF [kN] (Q)	1479.4	1	1479.4	5.65	0.063	No-Signif.	5.52
PT [s] (L)	80.6	1	80.6	0.31	0.603	No-Signif.	0.30
PT [s] (Q)	98.6	1	98.6	0.38	0.566	No-Signif.	0.37
RS (L) by AF(L)	542.9	1	542.9	2.07	0.209	No-Signif.	2.03
RS (L) by PT (L)	158.8	1	158.8	0.61	0.471	No-Signif.	0.59
AF (L) by PT (L)	23.0	1	23.0	0.09	0.779	No-Signif.	0.09
Error	1308.4	5	261.7				
Total sum of squares	26,764.5	14					

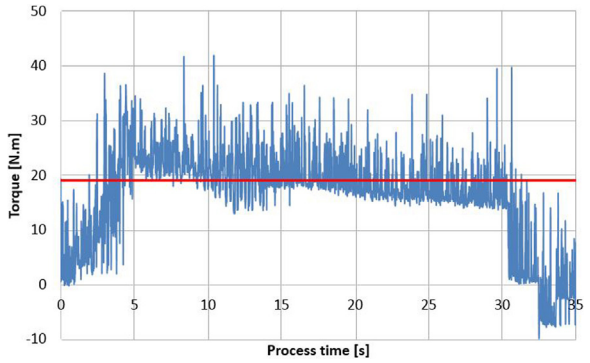

Fig. 16 – Typical torque curve of a HFDB tube to tube sheet. The red line presents the average value of the torque during the process.

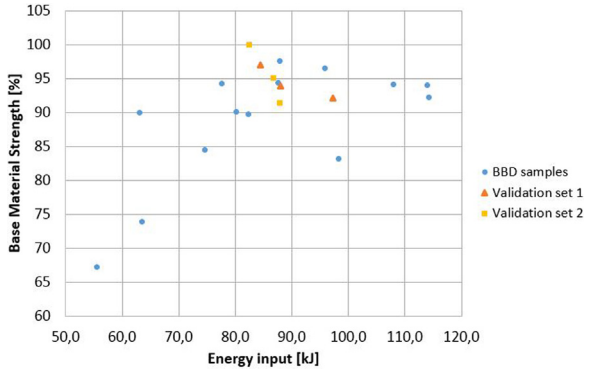

Fig. 17 – Energy input and resultant UTS of the weldments in relation to the base material strength.

the process. All other parameters or their interactions are shown to elicit non-significant responses. As already reported by several authors, the rotational speed is expected to be the parameter that has the greatest influences on temperature [16–19].

HFDB, like other thermo-mechanical processes, relies on a purely mechanical energy input during the welding process. It is possible to estimate the energy input using Eq. (2). Herein, E is the energy input in Joule, $\bar{M}$ is the torque average during the welding process in N m, n the rotational speed in Hertz and Δt is the difference between the final and initial process times in seconds. For the definition of the average value of torque, the torque curve of the process was acquired and its average value was calculated in accordance to the load cells present on the welding system. Fig. 16 shows a typical torque curve of the process, and the line in red indicates its average value.

$$E = 2\pi \times n \times \bar{M} \times \Delta t \quad (2)$$

If the energy input is plotted as a function of the strength of the welds, as shown in Fig. 16, it can be observed that there is a threshold necessary for achieving a weld with good mechanical properties. Fig. 17 indicates that the best results are in the range of 80–90 kJ. All validation samples, except one, are within this window. For energy inputs above this level, no further increase in UTS was found, and the strength of the weldments tended to decrease slightly. It is important to note that this can be concluded only for the window studied in this work. It can be expected that for significantly larger energy inputs, there will be softening and grain growth of the material leading to a decrease in the values of the mechanical properties of the welds [20–23]. Nevertheless, one feasible and easily implementable way to control the quality of the weldments, regarding their strength, is related to the control of the energy input during the process.

Thus, it is possible to conclude that it is not only the temperature that is necessary to achieve sound welds using HFDB. Although failure during pull out loading occurs mainly within the HAZ, the properties of the joint zone itself are obviously the determining factor for the joint strength. It is necessary to introduce a certain level of mechanical energy, which in this case is achieved by the axial force and rotational speed, as revealed by the BBD analyses. These factors determined the interaction of the tube and tube-sheet material with the tool, and in particular the material flow in the circumferential direction, i.e., the degree of plastic deformation. Although the axial force is not directly included in Eq. (2), it has a strong influence on the torque, thereby affecting the energy input.

In comparison to the conventional diffusion bonding process, the intense plastic deformation occurring in the welding region during HFDB provides sufficient energy for the occurrence of dynamic recrystallization [16,17,24,25]. The fact that the welding times in HFDB are significantly shorter than in conventional diffusion bonding processes is because of the introduction of lattice defects and the presence of additional grain boundaries, which can increase diffusion rates. The low recrystallized grain size in the weld region additionally leads to good mechanical material properties [26–29]. As previously shown in the statistical analysis of this study, axial force, followed by rotational speed, are the major parameters influencing the mechanical performance of the weldments.

5. Summary and conclusions

The BBD and the RSM were applied successfully to the optimization of the joining tubes to tube sheets for CWHE using HFDB. The following conclusions can be drawn from this study:

- The mechanical strength of the joints could be estimated by the application of a second-order regression model. The proposed regression model yielded a good fit to the experimental data.
- The best results were achieved by applying a rotational speed of 1500 min^{-1}, an axial force of 3 kN and a process time of 30 s. This process parameter set achieved an average of 95% UTS_{BM}.
- All samples were bubble leak tight. The most important criterion for this work was achieved for all process parameters chosen for this study.
- Axial force represented an influence of almost 63% on the analyzed ultimate tensile pull out strength followed by the influence of rotational speed that was approximately 23%.
- Higher axial forces were beneficial to the joint strength.

- There was no evident correlation between the maximum process temperature and mechanical performance, as investigated in this study, although an effect in the softening of the HAZ must be expected.
- The plastic deformation induced during the process introduced lattice defects and dynamic recrystallization, thus leading to additional grain boundaries through grain refinements. This facilitated diffusion that is considered to be the main contribution to the strength of the bonding zone.

Conflicts of interest

The authors declare no conflicts of interest.

REFERENCES

[1] Dethlefs A, Ross A, dos Santos JF, Wimmer G. Hybrid friction diffusion bonding of aluminium tube-to-tube-sheet connections in coil-wound heat exchangers. Mater Des 2014;60:7–12.

[2] Roos A [Doctoral Thesis] Grundlegende Untersuchung über ein neues Schweißverfahren namens HFDB (Hybrid Friction Diffusion Bonding). Ilmenau: Technischen Universität Ilmenau; 2010.

[3] dos Santos J, Roos A (Inventors). GKSS, assignee. Verfahren und Vorrichtung zum Herstellen einer Schweißverbindung zwischen den Oberflächen zweier flächiger Werkstücke. Patent Nr. EP1769877B1; 2007.

[4] Bergmann JP, Petzoldt F, Schürer R, Schneider S. Solid-state welding of aluminum to copper—case studies. Weld World 2013;57(4):541–50.

[5] dos Santos J, Roos A, Wimmer G (Inventors). GKSS, LINDE AG, assignee. Verfahren zum Verbinden von Rohrboden und Rohren im Rohrbündel-Wärmeübertrager. Patent Nr. EP2072173B1; 2013.

[6] Roos A, Alba DR, Hanke S, Wimmer G, dos Santos JF. Joining tube to tube sheet for coil wound heat exchangers by hybrid friction diffusion bonding. In: ASME 2015 – pressure vessels and piping conference. Boston, MA, USA: ASME; 2015. p.1–7.

[7] Box GE, Behnken DW. Some new three level designs for the study of quantitative variables. Technometrics 1960;2(4):455–75.

[8] Ferreira SLC, Bruns RE, Ferreira HS, Matos GD, David JM, Brandão GC, et al. Box–Behnken design: an alternative for the optimization of analytical methods. Anal Chim Acta 2007;597(2):179–86.

[9] Montgomery DC. Design and analysis of experiments. 3rd ed. New York: John Wiley & Sons; 1991.

[10] Box GE, Draper NR. Empirical model-building and response surfaces. New York: John Wiley & Sons; 1987.

[11] Myers RH, Montgomery DC, Anderson-Cook CM. Response surface methodology: process and product optimization using designed experiments. 3rd ed. New York: Wiley; 2009.

[12] AD 2000 Regelwerk. Berlin: Beuth Verlag; 2008.

[13] DIN EN 1593:1999-11. Non-destructive testing – leak testing – bubble emission techniques. Berlin: Deutsches Institut für Normung; 1999.

[14] Hirata T, Oguri T, Hagino H, Tanaka T, Chung SW, Takigawa Y, et al. Influence of friction stir welding parameters on grain size and formability in 5083 aluminum alloy. Mater Sci Eng A 2007;456(1):344–9.

[15] Sato YS, Urata M, Kokawa H, Ikeda K. Hall–Petch relationship in friction stir welds of equal channel angular-pressed aluminium alloys. Mater Sci Eng A 2003;354(1):298–305.

[16] Mishra RS, Ma ZJMS. Friction stir welding and processing. Mater Sci Eng R 2005;50(1–2):1–78.

[17] Węglowski MS. Friction stir processing – state of the art. Arch Civil Mech Eng 2018;18(1):114–29.

[18] Kumar R, Singh K, Pandey S. Process forces and heat input as function of process parameters in AA5083 friction stir welds. Trans Nonferrous Met Soc China 2012;22(2):288–98.

[19] Besharati-Givi MK, Asadi P. Advances in friction-stir welding and processing. Elsevier Science; 2014.

[20] Fiset M, Braunovic M, Galibois A. The effect of thermal cycling on grain growth in aluminum. Scr Metall 1971;5(4):325–8.

[21] Peel M, Stewer A, Preuss M, Withers PJ. Microstructure, mechanical properties and residual stresses as a function of welding speed in aluminium AA5083 friction stir welds. Acta Mater 2003;51(16):4791–801.

[22] Yazdipour A, Heidarzadeh A. Effect of friction stir welding on microstructure and mechanical properties of dissimilar Al 5083-H321 and 316L stainless steel alloy joints. J Alloys Compd 2016;680:595–603.

[23] Lin C-Y, Lui T-S, Chen L-H, Hung F-Y. Hall–Petch tensile yield stress and grain size relation of Al–5Mg–0.5 Mn alloy in friction-stir-processed and post-thermal-exposed conditions. Mater Trans 2014;55(2):357–62.

[24] Padhy GK, Wu CS, Gao S. Friction stir based welding and processing technologies – processes, parameters, microstructures and applications: a review. J Mater Sci Technol 2018;34(1):1–38.

[25] El-Danaf EA, El-Rayes MM, Soliman MS. Friction stir processing: an effective technique to refine grain structure and enhance ductility. Mater Des 2010;31(3):1231–6.

[26] Agarwal S, Krajewski PE, Briant CL. Texture development and dynamic recrystallization in AA5083 during superplastic forming at various strain rates. In: Advances in superplasticity and superplastic forming. TMS: Charlotte; 2004. p. 95–108.

[27] Sakai T, Belyakov A, Kaibyshev R, Miura H, Jonas JJ. Dynamic and post-dynamic recrystallization under hot, cold and severe plastic deformation conditions. Prog Mater Sci 2014;60:130–207.

[28] Cho J-H, Kim WJ, Lee CG. Evolution of microstructure and mechanical properties during friction stir welding of A5083 and A6082. Procedia Eng 2014;81:2080–5.

[29] Izadi H, Sandstrom R, Gerlich AP. Grain growth behavior and Hall–Petch strengthening in friction stir processed Al 5059. Metall Mater Trans A 2014;45(12):5635–44.